The ChlorON Series: Turn-on fluorescent protein sensors for imaging labile chloride in living cells

Jasmine N. Tutol[†§], Whitney S. Y. Ong[†§], Shelby M. Phelps[†], Weicheng Peng[†‡], Helen Goenawan[†], and Sheel C. Dodani[†*]

[†]Departments of Chemistry and Biochemistry and [‡]Biological Sciences, The University of Texas at Dallas, Richardson, TX 75080

[§]J.N.T and W.S.Y.O. contributed equally to this work.

[*]E-mail: sheel.dodani@utdallas.edu

Abstract

Chloride is a ubiquitous ion essential for regulating biological processes. Long thought to be just a counterion in biological systems, chloride is emerging as a vital anion that plays a major role in a range of diseases. The ability to visualize intracellular chloride has been enabled by fluorescent protein-based sensors. Although the yellow fluorescent protein from *Aequorea victoria*, and variants thereof, quench in the presence of chloride and other anions, they have provided valuable insights in biological studies and have established the benchmark for applying protein-based sensors for chloride. However, a single domain fluorescent protein sensor that generates a turn-on response to provide a spatial and temporal map of endogenous chloride has yet to be reported. Here, we highlight how mutagenesis of non-coordinating residues in the binding pocket of mNeonGreen has unlocked this new sensing capability. Our protein engineering efforts coupled with *in vitro* spectroscopy have led us to discover the ChlorON series as turn-on fluorescent sensors for chloride that operate at physiological pH. Fluorescence microscopy experiments with the ChlorON sensors reveal that cells have baseline levels of chloride, which could not have been directly observed with turn-off sensors. These advancements set the stage for visualizing endogenous chloride dynamics in real-time and uncovering new roles for chloride in biology.

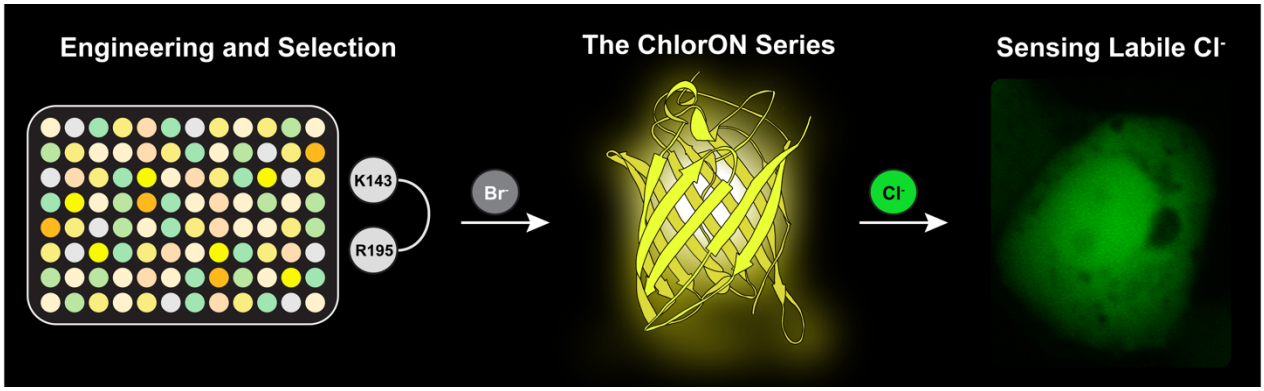

Introduction

Chloride is the most abundant physiological anion and is typically transported within cells through the activation of membrane-bound voltage or ligand-gated channels.[1] Traditionally, chloride is thought to function as a counterion during cellular processes such as signal transduction, acid-base homeostasis, and cell volume regulation.[2–4] Furthermore, chloride binding proteins and transporters are also expressed in all subcellular compartments, indicating that chloride could play a more vital role in organelle function. Dysregulation of chloride transport has been linked to a variety of diseases such as Bartter syndrome, hyperekplexia, cystic fibrosis, and epilepsy.[5–8] Along these lines, more recent studies on intracellular chloride channels and transporters have provided insights on emerging roles for chloride as a secondary messenger for gene expression, organelle acidification for lysosome function, and as an allosteric regulator for protein and enzyme activity.[9,10] This implies that cells have the capability of discerning and accessing various chloride pools during key biological processes.

Despite the emerging significance of chloride, the ability to study and manipulate endogenous chloride pools in a biological context is still underdeveloped. For example, our biological understanding of chloride has been facilitated by ion-selective electrode measurements, electrophysiological, and radioisotope labeling which perturb the cellular environment and do not provide molecular level insights on chloride dynamics in cells.[11,12] As a less invasive alternative, small molecule probes such as quinolinium and acridinium-based dyes have been developed to study and quantify intracellular chloride levels. However, these molecular scaffolds have low cell uptake, fluorescence quenching upon chloride binding, and low photostability. In recent years, there has been little progress for molecular-based sensors for chloride that can be applied in living cells. In parallel, genetically encoded fluorescent proteins can be used as biocompatible and non-invasive hosts for chloride that can also be targeted to various subcellular compartments. Even with only twenty proteinogenic amino acids, the natural biodiversity of fluorescent proteins can be harnessed using traditional protein engineering methods to sample, improve, and expand sensor function and properties, which is an advantage not easily accessible with molecular dyes.[13]

The majority of genetically encoded sensors for anions have been derived from green fluorescent protein (avGFP) from the jellyfish *Aequorea victoria*. Although avGFP is known not to bind chloride, it has been successfully engineered to generate the chloride-sensitive yellow variant (avYFP).[14] In general, these fluorescent proteins have a beta barrel structure with a single chromophore composed of three amino acids and a nearby pocket capable of chloride binding.[15] To illicit a fluorescence response, the chromophore equilibrium is shifted

between the non-fluorescent phenol and fluorescent phenolate states upon chloride binding. Subsequent studies have applied protein engineering methods around the chromophore and anion binding pocket to further enhance avGFP and avYFP photostability, protein folding, and binding affinity for chloride.[12,16–20] The engineered E^2GFP and avYFP-H148Q variants are well-known for elucidating the chloride binding mechanism. From these studies, chloride is known to interact with the T203Y residue, which also forms $\pi - \pi$ stacking interactions with the Y66 chromophore in avYFP-H148Q and E^2GFP (Figure S1); thus, resulting in a turn-off fluorescence response either through a shift in chromophore pK_a or static quenching, respectively. Outside of the GFP family, researchers have also converted red fluorescent protein mBeRFP from *Entacmaea quadricolor* into a ratiometric, turn-off sensor for chloride through different mutations, one of which is R205Y, which is analogous to T203Y in avYFP using site-directed mutagenesis (Figure S1).[21,22]

Given that fluorescence quenching upon chloride binding is also coupled to pH, rigorous pH controls are required for internal calibrations in mammalian cells. To account for this, E^2GFP and avYFP variants have been fused with chloride-insensitive fluorescent proteins to generate the ratiometric and/or FRET sensors such as ClopHensor, Clomeleon, and Cl-senor, to name a few.[18,23–28] These developments have allowed for ratiometric imaging of intracellular chloride and pH in mammalian cells, elucidating the mechanisms of chloride channels and transporters and facilitating drug discovery through high-throughput fluorescence screening. Although the fluorescent protein sensors discussed thus far have made major contributions to the neuroscience community, future biological discoveries for chloride can only be enabled through technological advancements in turn-on fluorescent imaging tools to provide spatial and temporal resolution for cellular chloride.

To this end, we sought to develop turn-on fluorescent protein-based sensors for imaging cellular chloride. To date, there are two examples of chloride-sensitive fluorescent proteins that have a turn-on response: phiYFP derived from jellyfish *Phialidium sp.* and mNeonGreen derived from the cephalochordate *Branchiostoma lanceolatum.*[29–32] phiYFP is a naturally occurring dimeric protein which is an excitation ratiometric and turn-on fluorescent sensor for chloride with binding affinity of ∼384 mM at pH 5.5.[31] On the other hand, mNeonGreen is a bright, monomeric turn-on fluorescent sensor for chloride with binding affinity of ∼10 mM at pH 4.5.[32] Given its higher binding affinity for chloride and monomeric state, mNeonGreen is a more attractive platform to engineer for cellular imaging applications. As shown in Figure 1A, the binding of chloride decreases the chromophore pK_a of mNeonGreen from the less fluorescent phenol chromophore to the highly fluorescent phenolate chromophore at pH 4.5. However, there is no response to chloride when measured at physiological pH.

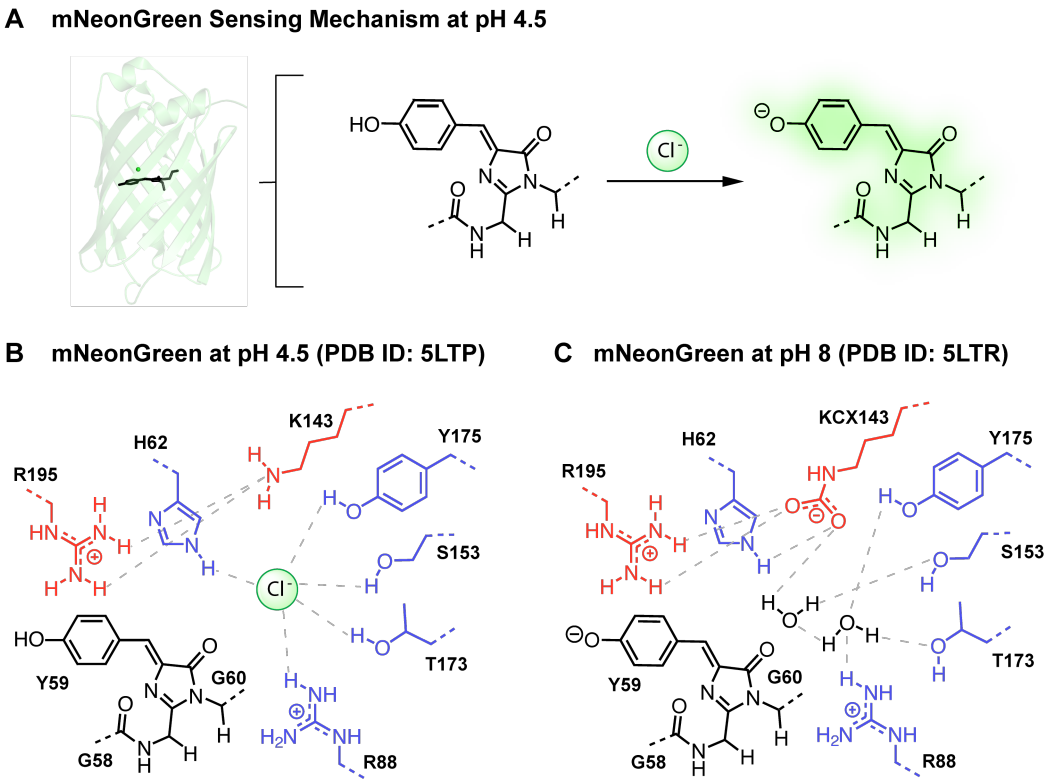

Figure 1. (A) The structure of mNeonGreen (mNG) bound to chloride (green sphere) at pH 4.5 (PDB ID: 5LTP) with the chromophore shown as black sticks (left panel). The chloride-dependent conversion of the chromophore from the non-fluorescent phenol to the fluorescent phenolate form, generating the turn-on response at pH 4.5 (right panel). Comparison of the chloride binding pockets in mNG crystallized (B) at pH 4.5 (PDB ID: 5LTP) and (C) pH 8.0 (PDB ID: 5LTR). For each schematic, the residues that make up the chromophore (black) and the coordinating (blue) and non-coordinating (red) residues within 4 Å of the chloride ion are shown. All residues are labeled with the single amino acid abbreviation and the position number. The hydrogen bond and electrostatic interactions less than 4 Å are shown as dashed lines.

To expand the operational pH of mNeonGreen, we first investigated the X-ray structures of mNeonGreen crystallized at pH 4.5 and pH 8 (Figure 1B and C).[33] Contrary to the chloride sensors derived from the GFP family where the chromophore contains a $\pi - \pi$ interaction with a tyrosine residue, mNeonGreen has an arginine residue (R195) above the phenol chromophore in place of the tyrosine. We have previously explored mutations on this site such as R195Y and observed that chloride binding increases the chromophore pK_as and results in a turn-off fluorescence response, indicating a relation that could be direct or indirect to anion binding response. Unlike the H62, R88, S153, T173, and Y175 residues that bind chloride, the R195 residue directly interacts with the K143 residue which could be involved in the outer sphere coordination of chloride (Figure 1B).[33] Interestingly, in the X-ray structures of mNeonGreen crystallized at pH 8, the K143 residue becomes carboxylated (KCX143) resulting in low chloride occupancy (30%) in the solid state and could provide one explanation for why mNeonGreen does not sense chloride near physiological pH (Figures 1C and S3).[33] Motivated by these observations, we hypothesized that by probing the mutational space of the two positions K143 and R195, we could identify a pair of mutations that could provide an increase in the operational pH and thus improve sensor properties.

Rational design of an anion binding pocket to be selective and sensitive can be challenging and time-consuming given that the rules of anion binding have yet to be defined. Alternatively, directed evolution can guide us to select for the desired function, in this case, a chloride-sensitive sensor. Given the large mutational space of proteins, a double-site saturation mutagenesis strategy was used to sample all possible mutations and select for sensors with desired properties. In this study, we have developed a workflow to engineer, screen, and identify a series of ChlorON sensors derived from mNeonGreen that have high turn-on fluorescence responses to chloride near physiological pH. Here, we investigated how the mutagenesis of the non-coordinating residues K143 and R195 in mNeonGreen can provide diverse binding pockets while tuning spectral properties and selecting for chloride turn-on response at physiological pH, rendering the ChlorON sensors more suitable for biological imaging applications.

Results

Mutagenesis of mNeonGreen and discovery of the ChlorON sensors

To explore the mutational space of K143 and R195 in mNeonGreen, we used a double site-saturation mutagenesis (DSSM) engineering strategy to sample all possible amino acid substitutions and combinations at both sites. In comparison to the other NNK and NNK/S engineering approaches, we chose to integrate the 22-c trick for the DSSM library to reduce codon redundancy and decrease our sampling size by at least 50%.[34] However, since K143 and R195 are far apart in the linear protein sequence, two sets of primers were designed for each site to minimize secondary interactions from long primers. In a single polymerase chain reaction, the DSSM library was generated and transformed in Escherichia coli (Figures 2 and S2, Tables S1 and S2).[34] To ensure that we have at least 95% library coverage (1,450 clones) at the K143 and R195 sites, 1,880 clones were sampled and expressed in a 96-well plate format.[34] As mentioned above, the native mNeonGreen chromophore pK_a is known to decrease from pK_a ~5.7 to pK_a ~4.7 with the addition of 25 mM chloride.[30,32] Thus, the library was carried out at pH 8 for optimal cell lysis using lysozyme to screen for variants with increased chromophore pK_as and gain chloride sensitivity at physiological pH.[35] For greater signal to noise ratios, the DSSM library was tested in the absence and presence of 100 mM sodium bromide to displace any residual chloride from the media. Under these conditions, the addition of bromide does not affect the parent mNeonGreen fluorescence (Table S3). Given that bromide has a larger ionic radius than chloride, we capitalized on the lack of selectivity in mNeonGreen, which has low apparent dissociation constants (K_d) for bromide ($K_d = 1.8 \pm 0.2$ mM) and chloride ($K_d = 9.8 \pm 0.3$ mM) at pH 4.5, to find new variants that could also bind chloride.[32] For cellular imaging application purposes, a threshold of > 4-fold turn-on was used to select for variants with large dynamic ranges. From the DSSM library, we have identified six mNeonGreen variants that fall within our selection criteria: K143Y/R195I (ca. 9.8-fold), K143R/R195L (ca. 9.2-fold), K143R/R195I (ca. 8.9-fold), K143W/R195L (ca. 7.3-fold), K143G/R195K (ca. 4.3- fold), and K143L/R195I (ca. 4.2-fold) (Figure S4, Table S3). To confirm the turn-on fluorescence response to halides, these variants were rescreened in cell lysate with 100 mM sodium chloride at pH 7 and 8. Although the turn-on responses for all variants were also responsive to 100 mM sodium chloride, the top three mNeonGreen variants that generated at least 25-fold turn-on responses to chloride at pH 7 contained the K143W/R195L (ChlorON-1), K143R/R195I (ChlorON-2), and K143R/R195L (ChlorON-3) mutations and were selected for full *in vitro* characterization (Table S3).

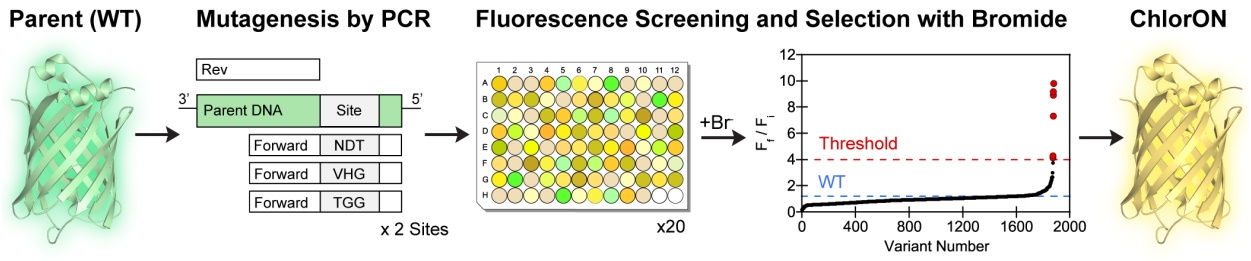

Figure 2. High-throughput protein engineering workflow developed to generate ChlorON sensors. Double-site saturation mutagenesis was carried out on selected sites in mNeonGreen and the libraries were screened with 100 mM bromide at pH 8. A 4-fold fluorescence turn-on threshold was applied on the library to select for variants for further characterization with chloride.

Spectroscopic characterization of the ChlorON sensors with chloride

Large-scale protein purification and size-exclusion chromatography preparations show that the ChlorON sensors are monomeric (Figure S5). To maintain protein stability in purified form, all protein stock solutions were stored in 50 mM phosphate buffer containing 50 mM sodium chloride at pH 7. For each experiment described below, the protein stock was further diluted 50-fold in a salt-free buffer to a final concentration of 1 mM chloride (see Supporting Information for details). Chloride titrations were first carried out at pH 7 to validate our library rescreening results and evaluate the applicability of the ChlorON sensors near physiological pH. The ChlorON-1, ChlorON-2, and ChlorON-3 absorption spectra contain two peaks at 400 nm and ∼480–485 nm that likely correspond to the phenol and phenolate chromophore states, respectively (Figure 3 , Table S4). With increasing chloride concentrations, the 400 nm absorption peak slightly increases while the ∼480–485 nm absorptions change in the opposite direction. Furthermore, the ChlorON-2 and ChlorON-3 absorption spectra reveal the rise of a new peak at 505 nm which could correspond to another orientation or state of the phenolate chromophore (Figure 3). Given the equilibrium between these two states, excitations were provided at 400 and 485 nm to investigate fluorescence response. Upon excitation at 400 nm, the fluorescence spectra of ChlorON-1, ChlorON-2, and ChlorON-3 show two emission maxima that correspond to the phenol chromophore at 460 nm and the phenolate chromophore at 515 nm. When excited at 485 nm, each ChlorON sensor has a single emission band centered at 515 nm (Figures 2 and S6–S8). Given the larger turn-on response, the relative fluorescence responses for the phenolate chromophore at 515 nm with $\lambda_{ex} = 485$ nm were evaluated from this point forward. Upon the addition of 200 mM sodium chloride, the ChlorON-1, ChlorON-2, and ChlorON-3 fluorescence increases 45-fold, 27-fold,

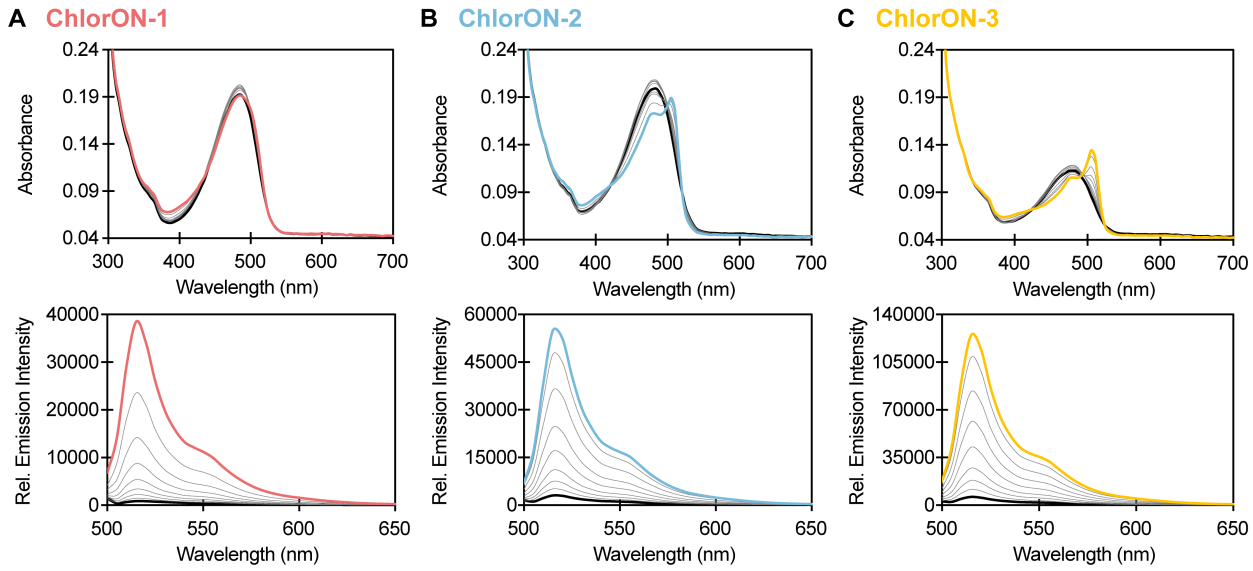

Figure 3. ChlorON-1/2/3 emit a turn-on fluorescence response to chloride at pH 7. Absorption (top row) and emission spectra (bottom row) of ∼10 μM (A) ChlorON-1, (B) ChlorON-2 and (C) ChlorON-3 in the presence of 1 (bold black), 2, 3.9, 6.9, 13.3, 25.5, 50, 99, and 197 mM (red, blue, and yellow, respectively) NaCl in 50 mM sodium phosphate buffer at pH 7. Excitation was provided at 485 nm, and the emission was collected from 500–650 nm. The average of four technical replicates from two protein preparations with standard error of the mean is reported (see Figures S6–S8).

and 20-fold, respectively, with the apparent dissociation constants (K_d) of 285 ± 59 mM, 55 ± 5 mM, and 30 ± 1 mM, respectively (Figures 3 and S6–S8, Table S4). The quantum yields of all three sensors are not measurable in the absence of chloride ($\phi < 0.01$), but in the presence of 197 mM chloride, the ChlorON-1 ($\phi \sim 0.03$), ChlorON-2 ($\phi \sim 0.09$), and ChlorON-3 ($\phi \sim 0.15$) quantum yields increase significantly (Figure S9, Table S4).

Since all fluorescent protein-based sensors for chloride are also sensitive to pH, chloride titrations were performed at pH 6 and 8 to assess how the fluorescence responses of the ChlorON sensors fluctuate as a function of pH. As described above, the phenolate to phenol ground state changes for ChlorON-1, ChlorON-2, and ChlorON-3 are more pronounced at pH 6 than at pH 7 and 8 which indicates that chloride could be influencing the chromophore equilibrium at lower pH (Figures S6–S8). The addition of chloride at pH 6 and excitation at 485 nm results in an increase in emission for ChlorON-1, ChlorON-2, and ChlorON-3 at 515 nm of 20-fold ($K_d = 39 \pm 5$ mM), 7.4-fold ($K_d = 7.5 \pm 1$ mM), and 6.2-fold ($K_d = 4.4 \pm 0.9$ mM), respectively (Figures 3 and S6–S8, Table S4). Interestingly, at pH 8, the ChlorON-1 absorbance spectra has a single peak at 485 nm that slightly broadens with chloride but does

not change in intensity (Figure S6C). At this pH, the ChlorON-1 chromophore is primarily in the phenolate state, but when excited at 485 nm, the ChlorON-1 emission increases 43.7-fold with a weak binding affinity for chloride (K_d) that could not be determined (Figure 6I). Under the same conditions, there is no phenol absorption at 400 nm for ChlorON-2 and ChlorON-3, but the addition of chloride causes a shift in the phenolate absorption from ∼480–485 nm to 505 nm with turn-on fluorescence responses and reduced chloride affinities of 21.4-fold and K_d = 228 ± 25 mM for ChlorON-2 (Figure S7), and 29-fold and K_d = 169 ± 79 mM for ChlorON-3 (Figure S8).

To further investigate the ChlorON sensing mechanism, pH titrations were carried out in the presence of 1 mM and 197 mM chloride to determine the chromophore pK_a for each sensor. As shown in Figure 4, the baseline fluorescence for ChlorON-1 minimally changes with increasing pH where the pK_a curve could not be fitted using the Henderson-Hasselbalch equation. However, in the presence of 197 mM chloride, ChlorON-1 fluorescence response demonstrated a classic sigmoidal shape with a chromophore pK_a of 6.0 ± 0.1 (Figure S10). Interestingly, unlike ChlorON-1, the ChlorON-2 and ChlorON-3 fluorescence responses are bell-shaped indicating the presence of two pK_as of the chromophore. This observation could arise from the deprotonation of a nearby residue as a function of pH. In the presence of chloride, the ChlorON-2 chromophore pK_as increases from 4.6 ± 0.1 and 6.1 ± 0.1 to 5.7 ± 0.1 and 7.6 ± 0.1 respectively (Figure S11). In a similar fashion, the ChlorON-3 pK_as of 4.8 ± 0.2 and 6.1 ± 0.2 increases to 6.0 ± 0.01 and 7.9 ± 0.1 respectively (Figure S12).

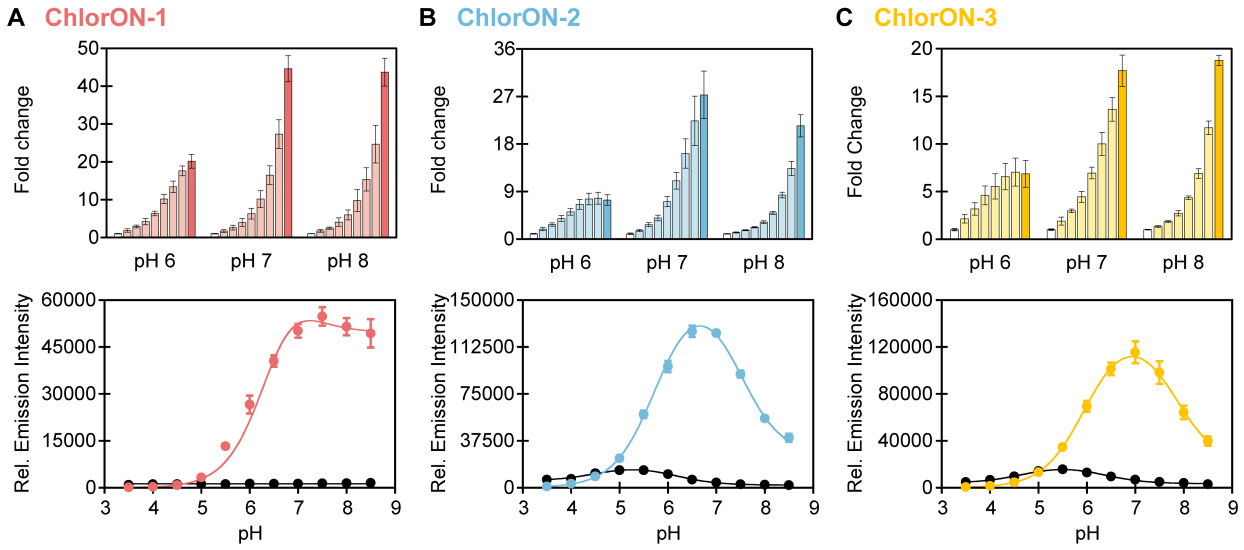

Figure 4. The ChlorONs can also sense chloride at different pH. The fluorescence response of (A) ChlorON-1, (B) ChlorON-2, and (C) ChlorON-3 to 1 (white bar, F_i), 2, 3.9, 6.9, 13.3, 25.5, 50, 99, and 197 mM (red, blue, and yellow bars, respectively) NaCl (F_f) at pH 6, 7, and 8 (first row) and to 1 (empty circles) and 197 mM (filled circles) NaCl from pH 3.5–8.5 (second row). All spectra were collected in 50 mM sodium acetate buffer from pH 3.5–5.5 and 50 mM sodium phosphate buffer from pH 5.5–8.5. Excitation was provided at 485 nm, and the emission response at 515 nm was analyzed. The average of four technical replicates from two protein preparations with standard error of the mean is reported (see Figures S6–S8, S10–S12).

Anion selectivity of the ChlorON sensors

Next, anion selectivity assays were carried out at pH 7. For all ChlorON sensors, minimal fluorescence changes were observed in the presence of phosphate, acetate, and citrate (Figures 5 and S13–S15). Titrations at pH 7 show that ChlorON-1 has a different turn-on response to each the following anions: chloride (45-fold) > bromide (26-fold) > iodide (2.6-fold) ≥ nitrate (2.2-fold) with apparent dissociation constants only measurable for chloride (K_d = 285 ± 59 mM) and bromide (K_d = 204 ± 38 mM). With the exception of iodide and nitrate, similar trends were observed for ChlorON-3 with the following anions: chloride (20-fold) > bromide (15-fold) > nitrate (7.9-fold) > iodide (3.8-fold). Interestingly, the binding affinities for ChlorON-3 are less differentiable between chloride (K_d = 30 ± 1 mM) and bromide (K_d = 32 ± 2 mM) as well as between nitrate (K_d = 54 ± 4 mM) and iodide (K_d = 48 ± 7 mM). For ChlorON-2, the trend of turn-on responses are as follows: bromide (30-fold) ≥ chloride (27-fold) > nitrate (9.1-fold) > iodide (6.3-fold). More notable differences are observed for

the ChlorON-2 binding affinities that do not follow the turn-on response trends: bromide ($K_d = 43 \pm 0.6$ mM) < chloride ($K_d = 55 \pm 5$ mM) < iodide ($K_d = 86 \pm 4$ mM) < nitrate ($K_d = 117 \pm 18$ mM) (Figures 5, S16–18 and Table S5). Interestingly, ChlorON-1 is not sensitive to sulfate, but absorbance shifts from the phenolate to phenol chromophore were observed for ChlorON-2 and ChlorON-3. These ground state shifts result in fluorescence quenching at 515 nm for ChlorON-2 (68%, $K_d = 17 \pm 2$ mM) and ChlorON-3 (87%, $K_d = 7.5 \pm 1$ mM) in the presence of 197 mM sulfate (Figure S19 and Table S5). Taken together, this data demonstrates how different mutations can have different effects on anion binding. Nevertheless, given the high abundance of chloride in cells, the ChlorON sensors still stand out as promising candidates for cellular applications.

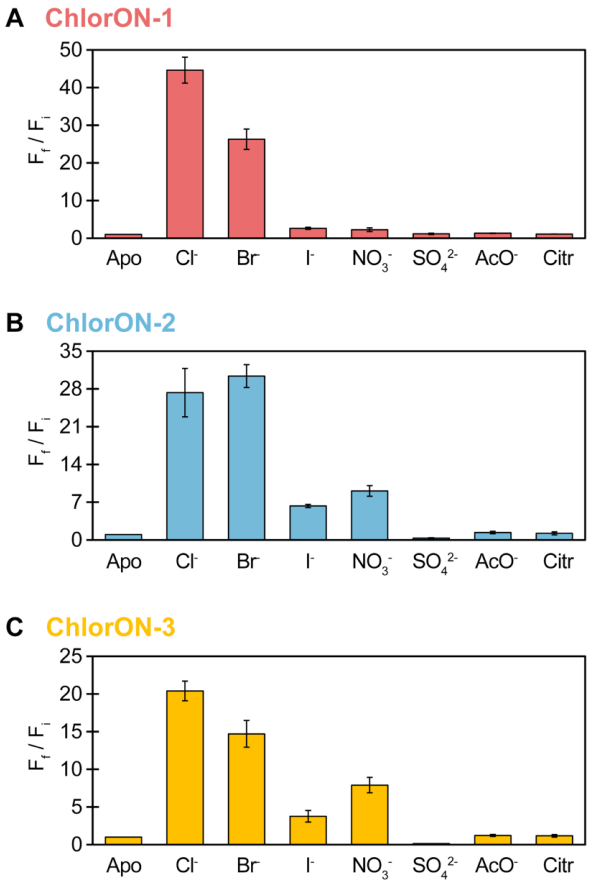

Figure 5. The ChlorON sensors are more selective for bromide and chloride in 50 mM sodium phosphate buffer at pH 7. Turn-on fluorescence response (F_f/F_i) of (A) ChlorON-1, (B) ChlorON-2 and (C) ChlorON-3 to 197 mM sodium chloride (Cl^-), bromide (Br^-), iodide (I^-), nitrate (NO_3^-), sulfate (SO_4^{2-}), acetate (AcO^-), and citrate (Citr). Excitation was provided at 485 nm, and the emission response at 515 nm was used to calculate F_f/F_i. The average of four technical replicates from two protein preparations with standard error of the mean is reported (see Figures S13–S19).

Validation of the ChlorON sensors using fluorescence microscopy

To further understand how the observed *in vitro* properties translate in live cells, fluorescence imaging experiments were conducted with ChlorON-1, ChlorON-2, and ChlorON-3. Thus, the genes encoding for the ChlorON sensors and mNeonGreen, which serves as our negative control, were synthesized in the pcDNA3.1(+) vector for protein expression in mammalian cells (Figure S20). Similar to the well-established methods for validating avYFP-H148Q-based turn-off sensors for chloride, the ChlorON-3 pcDNA was used to transfect Fischer Rat Thyroid (FRT) cells stably expressing the cystic fibrosis transmembrane conductance regulator protein (CFTR), a known chloride channel that becomes activated through phosphorylation by protein kinase A (PKA).[36,37] Treatment with forskolin (FSK) promotes the synthesis of cyclic adenosine monophosphate (cAMP) which triggers the PKA cell signaling pathway.[36,37] For this reason, FRT was selected as the model cell line because they do not have endogenous cAMP dependent chloride transporters.[38] To date, fluorescence-based assays have primarily used the avYFP-H148Q-I152L variant to measure CFTR activity through the exchange of extracellular chloride with iodide-containing buffers. This is because avYFP-H148Q-I152L was found to be more selective for iodide (K_d ∼2 mM) than chloride (K_d ∼85 mM).[17] Thus, the avYFP-H148Q-I152L fluorescence quenching with iodide, or lack thereof, can serve as a proxy for screening CFTR activators or inhibitors in compound drug libraries.[17,39–42]

FRT-CFTR cells transiently expressing the ChlorON sensors were incubated in a modified PBS buffer containing 137 mM sodium chloride to measure the baseline fluorescence signal (see Methods). CFTR activation was achieved through the addition of 20 μM FSK using a perfusion system which allowed us to repeatedly image the same fields of view. No change in the fluorescence response was observed for all protein sensors with FSK (Figure 6). The imaging solution was then exchanged with a modified PBS buffer containing FSK and 100 mM sodium iodide and 37 mM sodium chloride to control for ionic strength differences. Fluorescence quenching of ∼59%, ∼43%, and ∼51% was observed for ChlorON-1, ChlorON-2, and ChlorON-3, respectively, to indicate the import of iodide through CFTR and sodium iodide symporters expressed in FRT and CFTR-mediated export of chloride. Following this, the 137 mM sodium chloride buffer containing FSK was re-perfused to determine if the influx of chloride could restore the ChlorON fluorescence. As shown in Figure 6E, the ChlorON-1 fluorescence increases ca. 2.1-fold, ca. 1.5-fold for ChlorON-2, and ca. 1.8-fold for ChlorON-3. Under the same conditions, minor fluctuations in the mNeonGreen fluorescence were observed which could be due to cell volume changes associated with anion transport

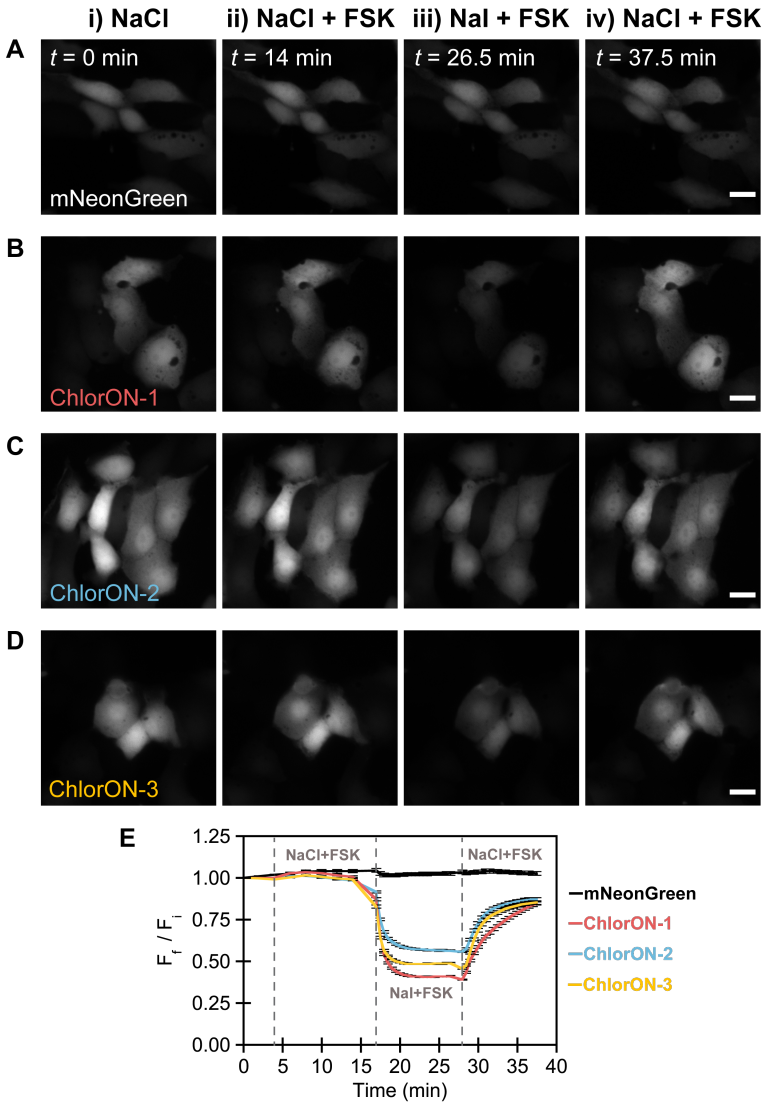

Figure 6. The ChlorON sensors report on labile chloride pools in live Fisher Rat Thyroid (FRT) cells overexpressing CFTR. Representative fluorescence images of cells expressing (A) mNeonGreen, (B) ChlorON-1, (C) ChlorON-2, and (D) ChlorON-3 in a modified PBS buffer supplemented with i) 137 mM NaCl at t = 0 min (F_i), ii) 137 mM NaCl and 20 μM forskolin (FSK, F_f) at t = 14 min, iii) 100 mM NaI, 37 mM NaCl, and 20 μM FSK (F_f) at t = 26.5 min, and iv) 137 mM NaCl and 20 μM FSK (Ff) at t = 37.5 min. Scale bars = 20 μm. Note: Exposure times are consistent within but variable between experiments. (E) Fluorescence response (F_f/F_i) of mNeonGreen (black line, n = 272 regions of interest (ROIs), ChlorON-1 (red line, n = 256 ROIs), ChlorON-2 (blue line, n = 230 ROIs), and ChlorON-3 (yellow line, n = 255 ROIs). All experiments were carried out in a modified PBS buffer (2.7 mM KCl, 0.7 mM $CaCl_2$, 1.1 mM $MgCl_2$, 1.5 mM KH_2PO_4, 8.1 mM Na_2HPO_4, and 10 mM glucose) at pH 7.4 with the corresponding supplement listed in each panel. The average fluorescence response (F_f/F_i) with standard error of the mean is reported for all ROIs from three biological replicates.

(Figures 6 and S21). To confirm that the observed fluorescence responses are indeed due to chloride and not pH, the dual excitation and pH-sensitive dye BCECF was used to stain FRT-CFTR cells. Undergoing the same treatments described above, the BCECF fluorescence remains unchanged (Figure S22). At the end of the experiment, the imaging solution was replaced with a pH 8 clamping buffer containing the K^+ ionophore valinomycin (5 μM) and the K^+/H^+ antiporter nigericin (5 μM) to confirm that BCECF is working properly. Equilibration of the intracellular pH to the external solution can be correlated to an increase in the BCECF fluorescence ratio (Figure S22). Thus, negligible pH changes were detected with the FSK treatments. Therefore, the observed turn-on fluorescence responses can be directly correlated to binding of chloride to ChlorON.

Discussion

Although all chloride sensitive fluorescent proteins with crystal structures have a definitive binding pocket with similar coordinating residues, the fluorescence response mechanism upon chloride binding may differ between variants even within the same family. For example, avGFP was converted into a turn-off sensor, E^2GFP, for chloride through the transplantation of the S65T and T203Y mutations. Structural and spectroscopic analysis demonstrate that E^2GFP senses chloride via static fluorescence quenching which can be attributed to its unique binding pocket where chloride forms interactions with T203Y, the peptide backbones of V68 and Q69, and a water molecule (Figure S1). In another study, avYFP-H148Q crystal structure showed that iodide directly interacts with the four hydrogen bond donating residues: Q69, R96, Q183, and Y203 (Figure S1). Through the $\pi - \pi$ stacking between Y203 and the Y66 chromophore, the binding of chloride to avYFP-H148Q increases the chromophore equilibrium (pK_a) to promote the non-fluorescent phenol state, resulting in a turn-off fluorescence response. Surprisingly, phiYFP, a homologue to the avYFP-H148Q sequence, was identified and reported as a turn-on fluorescent sensor for chloride even though multiple sequence alignment showed that these two proteins possess an identical chloride binding pocket (Figure S1).[31,43] A subsequent study showed that although the phiYFP chromophore pK_a increases with chloride, like in avYFP-H148Q, chloride titrations at pH 5.5 and time-resolved femtosecond transient absorption measurements confirm that phiYFP is an excitation-dependent, turn-on fluorescent sensor for chloride through an excited-state proton transfer process.[44] It is also worth mentioning that phiYFP is the first naturally occurring protein discovered sensitive to chloride with ratiometric properties. In contrast, the lack of

$\pi - \pi$ stacking to the chromophore in mNeonGreen indicates a different type of chloride sensing mechanism compared to the sensors mentioned above. In mNeonGreen, chloride binding shifts the chromophore equilibrium from the non-fluorescent phenol to fluorescent phenolate state resulting in a turn-on fluorescence response at acidic pH. In contrast, the ChlorON sensors emit large turn-on fluorescence responses at pH 7 despite minimal absorbance changes in ChlorON-1 and the appearance of new absorbance maxima in ChlorON-2 and ChlorON-3 with chloride (Figure 3). This suggests that different sensing mechanisms could be present in each of the three sensors.

Furthermore, the ground state differences between ChlorON-1 and ChlorON-3 are notable even though they only differ by only one mutation. This indicates that the mutation at K143 is important in the chloride binding event and response. Given that K143R and K143W are both capable of being hydrogen bond donors, we speculate that the now-replaced lysine residue prevents the carboxylation of the 143 residue, as was observed in mNeonGreen, thus allowing chloride to bind (Figure 1C). Additionally, in comparison to ChlorON-1, ChlorON-2 and ChlorON-3 both have the K143R mutation and stronger chloride binding affinities for chloride which could stem from the introduction of a positively charged arginine residue that is capable of forming electrostatic interactions with chloride. Since all three sensors have either a leucine or isoleucine residue at the R195 position, these hydrophobic residues could contribute to the steric effect, resulting in selectivity for anion size and shape. For example, the ChlorONs have larger turn-on responses for chloride over iodide which is a trend not commonly found in other fluorescent protein-based sensors, including mNeonGreen.[15–17,23,32,45,46]

The bell shaped curves of ChlorON-2 and ChlorON-3 showed that the fluorescence responses increased as a function of pH before declining after pH 7.5 (Figure 4). This data suggests the presence of a second pK_a which can be attributed to the K143R mutations in ChlorON-2 and ChlorON-3. This observation is not seen in ChlorON-1, indicating that the K143W mutation does not contribute to this phenomenon. We investigated this further by looking at the position of K143 in the crystal structure of mNeonGreen and found that a nearby residue H62 (within 4 Å) could be deprotonated with increased pH and could affect the excited state properties of the chromophore. Although the pK_a of a histidine residue is ∼6–7, it is known that pH can influence the global protein structure and protein microenvironments. In this case, we speculate that the effect of H62 could be interacting with the arginine side chain in K143R. However, additional mechanistic studies of the ChlorON-2 and ChlorON-3 using time-resolved spectroscopy are beyond the scope of this study. Nonetheless, there is still a large turn-on response from pH 5.5 to 8 for all ChlorON sensors. This is

especially advantageous for cell imaging applications since the transport of chloride is known to cause intracellular pH fluctuations.

In summary, we have engineered the first monomeric, turn-on fluorescent protein capable of chloride sensing at physiological pH that is compatible for cell imaging assays to aid in expanding the current knowledge for the roles of chloride in cellular processes. Overall, our structurally guided engineering strategy has allowed us to effectively sample the mutational space in mNeonGreen, screen for halide sensitivity at pH 8, and discover variants with desired properties (Figure 2). With bromide used as the initial selection pressure to minimize background interference, the selected sensors were sensitive to both bromide and chloride. However, bromide is not abundant in biological systems; thus, minimal interference can be expected when using the ChlorON sensors in cells. Our motivation for developing the engineered ChlorON sensors is to improve upon existing platforms to monitor the spatial and temporal dynamics of chloride in cells. Indeed our imaging studies using the BCECF pH dye confirm that the observed turn-on fluorescence responses can be directly correlated to binding of chloride to the ChlorON sensors even in the presence of different cellular analytes. In comparison to the *in vitro* results, we suspect that the attenuated turn-on response for the ChlorON sensors in cells could be due to a threshold of exchange for chloride influx and iodide efflux.[17] Nevertheless, the imaging results show that the ChlorON sensors can equilibrate with endogenous and exchangeable chloride pools given that the ChlorON fluorescence can be restored near baseline levels post iodide-chloride exchange. Furthermore, the quenched fluorescence output from all three sensors is still detectable even in the presence of iodide which contrasts the established turn-off chloride sensors. When bound to chloride, the ChlorON sensors can access larger dynamic ranges that is only limited by the maximum threshold of chloride transport in live, intact cells. Taken together, we demonstrate the advantage of using turn-on fluorescent sensors to maintain spatial resolution in order to visualize subtle changes in cell dynamics. Additionally, we can expand the biological applications for the ChlorON sensors using targeting sequences to investigate chloride in subcellular compartments.

Conclusion and Future Directions

To close, we have highlighted our ability to sample the protein sequence space in mNeonGreen, which had limited function at physiological pH, using protein engineering methods and transform it into a series of turn-on fluorescent sensors for chloride (ChlorON). However, even with 20 amino acids, accumulated mutations create exponentially large sequence

space to be sampled. Therefore, laboratory guided site-saturation mutagenesis coupled with high throughput screening can generate a sensor with desired properties. Here, we have discussed how the accumulation and combination of mutations found at K143 and R195 not only translate to large dynamic ranges for chloride but also varying affinities for chloride and other anions in ChlorON-1, ChlorON-2, and ChlorON-3.

From the supramolecular chemistry point of view, the challenge in chloride sensor development is due to the inherent difficulty of overcoming the thermodynamic barrier for chloride desolvation and recognition. On the other hand, with every mutation that we select for in newly engineered proteins, the resulting variants may have different properties and sensing mechanisms as demonstrated in this study. Rational design of mutational space while keeping targeted anion binding in mind is not only challenging but time consuming. To bypass this and to explore all possible mutations, directed evolution is used to prioritize sensor functionality before mechanistic details can be studied. As part of a larger program to explore labile chloride pools and their contributions to cell physiology and pathology, we aim to develop genetically encoded turn-on sensors with ideal sensing capabilities such as improved sensitivity and selectivity to chloride at physiological pH. Future directions include computational modeling, X-ray crystallography, and ultrafast spectroscopy to elucidate the chloride sensing mechanisms found in the ChlorON sensors and provide insight on how to further improve the next generation of sensors. This will allow us to establish the criteria required to build functional tools and diversify the imaging toolkit for chloride. These technological advancements will not only facilitate the imaging of chloride dynamics in real-time but also accelerate the discovery of new roles for chloride in biology.

Acknowledgements

The authors acknowledge members of the Dodani Lab for helpful discussions. The FRT-CFTR cells were kindly gifted by Dr. Jeong Hong from Emory University and the Cystic Fibrosis Foundation. S.C.D. acknowledges support for this work from UT Dallas, the Welch Foundation (AT-1918-20170325, AT-2060-20210327), and the National Institute of General Medical Sciences of the National Institutes of Health (R35GM128923). This study is the sole responsibility of the authors and does not represent the views of the funding sources.

Author contributions

S.C.D. designed the research project. J.N.T., W.S.Y.O., S.M.P, W.P., H.G., and S.C.D. designed and carried out the experiments. J.N.T, W.S.Y.O, and S.C.D. wrote the manuscript with input from all authors.

Conflicts of interest

A provisional patent application has been filed for the ChlorON sensors.

ORCID

Jasmine N. Tutol: 0000-0001-8493-4203
Whitney S. Y. Ong: 0000-0001-9821-9972
Shelby M. Phelps: 0000-0002-2885-189X
Weicheng Peng: 0000-0002-1481-625X
Helen Goenawan: 0000-0001-7842-0150
Sheel C. Dodani: 0000-0003-0271-6080

REFERENCES

[1] Reuter, D.; Zierold, K.; Der, W. H. S.; Frings, S. A Depolarizing Chloride Current Contributes to Chemoelectrical Transduction in Olfactory Sensory Neurons In Situ. *J. Neurosci.* **1998**, *18*, 6623–6630.

[2] Verkman, A. S. Development and biological applications of chloride-sensitive fluorescent indicators. *Am. J. Physiol.: Cell Physiol.* **1990**, *259*, C375–C388.

[3] Suzuki, M.; Morita, T.; Iwamoto, T. Diversity of Cl-Channels. *Cell. Mol. Life Sci.* **2006**, *63*, 12.

[4] Puljak, L.; Kilic, G. Emerging roles of chloride channels in human diseases. *Biochim. Biophys. Acta, Mol. Basis Dis.* **2006**, *1762*, 404–413.

[5] Verkman, A. S.; Galietta, L. J. V. Chloride channels as drug targets. *Nat. Rev. Drug Discovery* **2009**, *8*, 153–171.

[6] Planells-Cases, R.; Jentsch, T. J. Chloride channelopathies. *Biochim. Biophys. Acta, Mol. Basis Dis.* **2009**, *1792*, 173–189.

[7] Gagnon, M. et al. Chloride extrusion enhancers as novel therapeutics for neurological diseases. *Nat. Med.* **2013**, *19*, 1524–1528.

[8] Peretti, M.; Angelini, M.; Savalli, N.; Florio, T.; Yuspa, S. H.; Mazzanti, M. Chloride channels in cancer: Focus on chloride intracellular channel 1 and 4 (CLIC1 AND CLIC4) proteins in tumor development and as novel therapeutic targets. *Biochim. Biophys. Acta, Biomembr.* **2015**, *1848*, 2523–2531.

[9] Valdivieso, Á. G.; Clauzure, M.; Massip-Copiz, M.; Santa-Coloma, T. A. The Chloride Anion Acts as a Second Messenger in Mammalian Cells - Modifying the Expression of Specific Genes. *Cell. Physiol. Biochem.* **2016**, *38*, 49–64.

[10] Valdivieso, Á. G.; Santa-Coloma, T. A. The chloride anion as a signalling effector. *Biol. Rev.* **2019**, *94*, 1839–1856.

[11] Geddes, C. D. Optical halide sensing using fluorescence quenching: theory, simulations and applications - a review. *Meas. Sci. Technol.* **2001**, *12*, R53–R88.

[12] Zajac, M.; Chakraborty, K.; Saha, S.; Mahadevan, V.; Infield, D. T.; Accardi, A.; Qiu, Z.; Krishnan, Y. What biologists want from their chloride reporters – a conversation between chemists and biologists. *J. Cell Sci.* **2020**, *133*.

[13] Tutol, J. N.; Lee, J.; Chi, H.; Faizuddin, F. N.; Abeyrathna, S. S.; Zhou, Q.; Morcos, F.; Meloni, G.; Dodani, S. C. A single point mutation converts a proton-pumping rhodopsin into a red-shifted, turn-on fluorescent sensor for chloride. *Chem. Sci.* **2021**, *12*, 5655–5663.

[14] Wachter, R. M.; Remington, S. J. Sensitivity of the yellow variant of green fluorescent protein to halides and nitrate. *Curr. Biol.* **1999**, *9*, R628–R629.

[15] Wachter, R. M.; Yarbrough, D.; Kallio, K.; Remington, S. Crystallographic and energetic analysis of binding of selected anions to the yellow variants of green fluorescent protein 1 1Edited by D. C. Rees. *J. Mol. Biol.* **2000**, *301*, 157–171.

[16] Jayaraman, S.; Haggie, P.; Wachter, R. M.; Remington, S.; Verkman, A. Mechanism and Cellular Applications of a Green Fluorescent Protein-based Halide Sensor. *J. Biol. Chem.* **2000**, *275*, 6047–6050.

[17] Galietta, L. J.; Haggie, P. M.; Verkman, A. Green fluorescent protein-based halide indicators with improved chloride and iodide affinities. *FEBS Lett.* **2001**, *499*, 220–224.

[18] Markova, O.; Mukhtarov, M.; Real, E.; Jacob, Y.; Bregestovski, P. Genetically encoded chloride indicator with improved sensitivity. *J. Neurosci. Methods* **2008**, *170*, 67–76.

[19] Zhong, S.; Navaratnam, D.; Santos-Sacchi, J. A Genetically-Encoded YFP Sensor with Enhanced Chloride Sensitivity, Photostability and Reduced pH Interference Demonstrates Augmented Transmembrane Chloride Movement by Gerbil Prestin (SLC26a5). *PLoS ONE* **2014**, *9*, e99095.

[20] Baek, K.; Ji, K.; Peng, W.; Liyanaarachchi, S. M.; Dodani, S. C. The design and evolution of fluorescent protein-based sensors for monoatomic ions in biology. *Protein Eng., Des. Sel.* **2021**, *34*.

[21] Yang, J.; Wang, L.; Yang, F.; Luo, H.; Xu, L.; Lu, J.; Zeng, S.; Zhang, Z. mBeRFP, an Improved Large Stokes Shift Red Fluorescent Protein. *PLoS ONE* **2013**, *8*, e64849.

[22] Salto, R.; Giron, M. D.; Puente-Muñoz, V.; Vilchez, J. D.; Espinar-Barranco, L.; Valverde-Pozo, J.; Arosio, D.; Paredes, J. M. New Red-Emitting Chloride-Sensitive Fluorescent Protein with Biological Uses. *ACS Sens.* **2021**, *6*, 2563–2573.

[23] Kuner, T.; Augustine, G. J. A Genetically Encoded Ratiometric Indicator for Chloride. *Neuron* **2000**, *27*, 447–459.

[24] Bizzarri, R.; Arcangeli, C.; Arosio, D.; Ricci, F.; Faraci, P.; Cardarelli, F.; Beltram, F. Development of a Novel GFP-based Ratiometric Excitation and Emission pH Indicator for Intracellular Studies. *Biophys. J.* **2006**, *90*, 3300–3314.

[25] Arosio, D.; Ricci, F.; Marchetti, L.; Gualdani, R.; Albertazzi, L.; Beltram, F. Simultaneous intracellular chloride and pH measurements using a GFP-based sensor. *Nat. Methods* **2010**, *7*, 516–518.

[26] Raimondo, J. A genetically-encoded chloride and pH sensor for dissociating ion dynamics in the nervous system. *Front. Cell. Neurosci.* **2013**, *7*.

[27] Grimley, J. S.; Li, L.; Wang, W.; Wen, L.; Beese, L. S.; Hellinga, H. W.; Augustine, G. J. Visualization of Synaptic Inhibition with an Optogenetic Sensor Developed by Cell-Free Protein Engineering Automation. *J. Neurosci.* **2013**, *33*, 16297–16309.

[28] Paredes, J. M.; Idilli, A. I.; Mariotti, L.; Losi, G.; Arslanbaeva, L. R.; Sato, S. S.; Artoni, P.; Szczurkowska, J.; Cancedda, L.; Ratto, G. M.; Carmignoto, G.; Arosio, D. Synchronous Bioimaging of Intracellular pH and Chloride Based on LSS Fluorescent Protein. *ACS Chem. Biol.* **2016**, *11*, 1652–1660.

[29] Shagin, D. A.; Barsova, E. V.; Yanushevich, Y. G.; Fradkov, A. F.; Lukyanov, K. A.; Labas, Y. A.; Semenova, T. N.; Ugalde, J. A.; Meyers, A.; Nunez, J. M.; Widder, E. A.; Lukyanov, S. A.; Matz, M. V. GFP-like Proteins as Ubiquitous Metazoan Superfamily: Evolution of Functional Features and Structural Complexity. *Mol. Biol. Evol.* **2004**, *21*, 841–850.

[30] Shaner, N. C.; Lambert, G. G.; Chammas, A.; Ni, Y.; Cranfill, P. J.; Baird, M. A.; Sell, B. R.; Allen, J. R.; Day, R. N.; Israelsson, M.; Davidson, M. W.; Wang, J. A bright monomeric green fluorescent protein derived from Branchiostoma lanceolatum. *Nat. Methods* **2013**, *10*, 407–409.

[31] Tutol, J. N.; Peng, W.; Dodani, S. C. Discovery and Characterization of a Naturally Occurring, Turn-On Yellow Fluorescent Protein Sensor for Chloride. *Biochemistry* **2019**, *58*, 31–35.

[32] Tutol, J. N.; Kam, H. C.; Dodani, S. C. Identification of mNeonGreen as a pH-Dependent, Turn-On Fluorescent Protein Sensor for Chloride. *ChemBioChem* **2019**, cbic.201900147.

[33] Clavel, D.; Gotthard, G.; von Stetten, D.; Sanctis, D. D.; Pasquier, H.; Lambert, G. G.; Shaner, N. C.; Royant, A. Structural analysis of the bright monomeric yellow-green fluorescent protein mNeonGreen obtained by directed evolution. *Acta Crystallogr., Sect. D: Struct. Biol.* **2016**, *72*, 1298–1307.

[34] Kille, S.; Acevedo-Rocha, C. G.; Parra, L. P.; Zhang, Z.-G.; Opperman, D. J.; Reetz, M. T.; Acevedo, J. P. Reducing Codon Redundancy and Screening Effort of Combinatorial Protein Libraries Created by Saturation Mutagenesis. *ACS Synth. Biol.* **2013**, *2*, 83–92.

[35] Banerjee, P.; Keener, K.; Lukito, V. Influence of carbon dioxide on the activity of chicken egg white lysozyme. *Poult. Sci.* **2011**, *90*, 889–895.

[36] Moran, O.; Zegarra-Moran, O. On the measurement of the functional properties of the CFTR. *J. Cystic Fibrosis* **2008**, *7*, 483–494.

[37] Hwang, T.-C.; Kirk, K. L. The CFTR Ion Channel: Gating, Regulation, and Anion Permeation. *Cold Spring Harbor Perspect. Med.* **2013**, *3*.

[38] Sheppard, D. N.; Carson, M. R.; Ostedgaard, L. S.; Denning, G. M.; Welsh, M. J. Expression of cystic fibrosis transmembrane conductance regulator in a model epithelium. *Am. J. Physiol.: Lung Cell. Mol. Physiol.* **1994**, *266*, L405–L413.

[39] Galietta, L. V. J.; Jayaraman, S.; Verkman, A. S. Cell-based assay for high-throughput quantitative screening of CFTR chloride transport agonists. *Am. J. Physiol.: Cell Physiol.* **2001**, *281*, C1734–C1742.

[40] Fiore, M.; Cossu, C.; Capurro, V.; Picco, C.; Ludovico, A.; Mielczarek, M.; Carreira-Barral, I.; Caci, E.; Baroni, D.; Quesada, R.; Moran, O. Small molecule-facilitated anion transporters in cells for a novel therapeutic approach to cystic fibrosis. *Br. J. Pharmacol.* **2019**, *176*, 1764–1779.

[41] Li, H.; Valkenier, H.; Thorne, A. G.; Dias, C. M.; Cooper, J. A.; Kieffer, M.; Busschaert, N.; Gale, P. A.; Sheppard, D. N.; Davis, A. P. Anion carriers as potential treatments for cystic fibrosis: transport in cystic fibrosis cells, and additivity to channel-targeting drugs. *Chem. Sci.* **2019**, *10*, 9663–9672.

[42] Gianotti, A.; Capurro, V.; Delpiano, L.; Mielczarek, M.; García-Valverde, M.; Carreira-Barral, I.; Ludovico, A.; Fiore, M.; Baroni, D.; Moran, O.; Quesada, R.; Caci, E. Small Molecule Anion Carriers Correct Abnormal Airway Surface Liquid Properties in Cystic Fibrosis Airway Epithelia. *Int. J. Mol. Sci.* **2020**, *21*.

[43] Pletneva, N. V.; Pletnev, V. Z.; Souslova, E.; Chudakov, D. M.; Lukyanov, S.; Martynov, V. I.; Arhipova, S.; Artemyev, I.; Wlodawer, A.; Dauter, Z.; Pletnev, S. Yellow fluorescent protein phiYFPv (*Phialidium*): structure and structure-based mutagenesis. *Acta Crystallogr., Sect. D: Biol. Crystallogr.* **2013**, *69*, 1005–1012.

[44] Chen, C.; Tutol, J. N.; Tang, L.; Zhu, L.; Ong, W. S. Y.; Dodani, S. C.; Fang, C. Excitation ratiometric chloride sensing in a standalone yellow fluorescent protein is powered by the interplay between proton transfer and conformational reorganization. *Chem. Sci.* **2021**, *12*, 11382–11393.

[45] Arosio, D.; Garau, G.; Ricci, F.; Marchetti, L.; Bizzarri, R.; Nifosì, R.; Beltram, F. Spectroscopic and Structural Study of Proton and Halide Ion Cooperative Binding to GFP. *Biophys. J.* **2007**, *93*, 232–244.

[46] Bregestovski, P. Genetically encoded optical sensors for monitoring of intracellular chloride and chloride-selective channels activity. *Front. Mol. Neurosci.* **2009**, *2*.